



## Research Article

George Baffour Pipim, Mallikarjun Sharada\* and Anna I. Krylov\*

# Photophysical properties of functionalized terphenyls and implications to photoredox catalysis

<https://doi.org/10.1515/pac-2025-0560>

Received July 2, 2025; accepted August 8, 2025

**Abstract:** Developing efficient organic photoredox catalysts is essential for advancing sustainable CO<sub>2</sub> conversion technologies. This paper investigates the photophysical properties of oligo-*p*-phenylenes (OPP-*n*), with a focus on *p*-terphenyl (OPP-3), and its functionalized derivatives to identify structural features that may enhance their photocatalytic potential. We examine how symmetric and asymmetric terminal substitutions affect excitation energies, oscillator strengths, exciton characteristics, and fluorescence. Our results show that push–pull derivatives have significantly lower excitation energies and larger oscillator strengths, promoting efficient radical anion generation. These derivatives also exhibit longer fluorescence lifetimes, which may improve the probability of productive interactions with sacrificial electron donors. Exciton analysis reveals that asymmetric substitutions introduce charge-transfer character, whereas higher oligomers maintain tightly bound excitons with limited delocalization. Overall, functionalized OPP-*n* chromophores, especially push–pull derivatives of OPP-3, demonstrate favorable optical and excitonic properties for photoredox catalysis, making them promising candidates for CO<sub>2</sub> reduction and hydrogen evolution applications.

**Keywords:** CO<sub>2</sub> conversion; exciton; photoredox catalysis; quantum science and technology; terphenyls.

## Introduction

The emission of carbon dioxide (CO<sub>2</sub>) globally has doubled over the past three decades and, given the current rates of fossil fuel consumption, it is estimated to triple in the next two decades. High concentrations of CO<sub>2</sub> are anticipated to increase the average global temperature with negative effects on the environment.<sup>1–6</sup> CO<sub>2</sub> photoreduction, which promises to mimic photosynthesis and mitigate the greenhouse effect, has received significant attention over the past few decades.<sup>7–14</sup> Photoredox catalysis has potential as a sustainable alternative to conventional, energy-intensive, thermally activated reaction pathways by accessing highly reactive radical states through photo-induced excitation and quenching.<sup>15–18</sup> Experimental studies have demonstrated the efficient photoreduction of CO<sub>2</sub> using organic chromophores known as oligo-*p*-phenylenes (OPP-*n*, where *n* denotes the number of phenylene units), yielding products such as formate, amino acids, and hydrocarboxylated styrene.<sup>19–21</sup>

---

**Article note:** A collection of invited papers to celebrate the UN's proclamation of 2025 as the International Year of Quantum Science and Technology.

---

\***Corresponding authors:** Mallikarjun Sharada, Department of Chemistry, University of Southern California, Los Angeles, CA 90089, USA; and Mork Family Department of Chemical Engineering and Materials Science, University of Southern California, Los Angeles, CA 90089, USA, e-mail: ssharada@usc.edu; and Anna I. Krylov, Department of Chemistry, University of Southern California, Los Angeles, CA 90089, USA, e-mail: krylov@usc.edu. <https://orcid.org/0000-0001-6788-5016>

George Baffour Pipim, Department of Chemistry, University of Southern California, Los Angeles, CA 90089, USA. <https://orcid.org/0000-0002-4700-8005>

Figure 1 shows the proposed photoredox catalytic cycle for this transformation. The catalytic scheme begins with the photoexcitation of OPP-*n* to its singlet excited state upon UV–Vis irradiation at 4.28 eV (290 nm).<sup>21</sup> The electronically excited state, [OPP-*n*]\*, has a substantially higher electron affinity and a lower ionization energy than the ground state OPP-*n* because in the excited state the HOMO and LUMO are half-filled.<sup>22–25</sup> Consequently, [OPP-*n*]\* can interact with sacrificial electron donors (in this case, triethylamine, Et<sub>3</sub>N or TEA) – leading to either excited-state quenching via electron transfer or the formation of an excited-state complex (exciplex) in low dielectric solvents that decays back to neutral ground-state fragments.<sup>26–31</sup> The radical anion is an effective reducing agent and can carry out a single electron reduction of CO<sub>2</sub>.<sup>31,32</sup>

There is a strong need for rational photoredox catalyst design as the phenylene oligomers examined thus far typically exhibit low turnover numbers on account of deactivation via photo-Birch reduction and carboxylation competing with electron transfer to CO<sub>2</sub>. In addition to being soluble in the solvent of choice, the ability of these catalysts to convert carbon dioxide to value-added products such as formic acid depends on their optical properties. An ideal photoredox catalyst should be excitable by visible light, have large oscillator strength, and be efficiently quenched by a sacrificial electron donor to generate a radical anion. The resulting radical anion should also possess high oxidizing potential that favor subsequent electron transfer to CO<sub>2</sub>. Studies that explicitly compared the catalytic abilities of the different oligomers for photoreduction found that the *p*-terphenyl and *p*-tetraphenyl are more effective than other oligomers and interestingly more active than the *p*-phenylene polymer.<sup>19,21</sup>

In this paper, we investigate the optical properties of oligo-*p*-phenylenes (OPP-*n*) to identify the key structural and electronic factors that can impact catalytic performance. We explore the potential to tune these properties through terminal substitution with electron-donating and electron-withdrawing groups, aiming to lower excitation energies and enhance photoredox activity. To understand how substitution affects the electronic properties of these chromophores, we employ exciton descriptors to analyze changes in exciton localization, delocalization, and charge-transfer character. We also examine changes in the excited-state structure and fluorescence behavior of the substituted catalysts relative to the parent catalyst, providing further insight into their suitability for photoredox applications.

## Computational details

All calculations were performed with the density functional theory (DFT) and time-dependent density functional theory (TD-DFT) using the Q-Chem software package.<sup>33</sup> We used the range-separated  $\omega$ B97X-D3 and LRC- $\omega$ PBE functionals, as they are among the best-performing functionals for describing the excited-state properties.<sup>34–36</sup> In particular, range-separation is important for the correct treatment of charge-transfer character. Ground-state structures were optimized with  $\omega$ B97X-D3/aug-cc-pVDZ in cyclohexane, followed with frequency calculations to verify that the obtained structures corresponded to the minima. We computed vertical excitation energies of the molecules as the electronic energy difference between the ground state and corresponding excited state at the ground state equilibrium geometry using LRC- $\omega$ PBE/aug-cc-pVDZ.

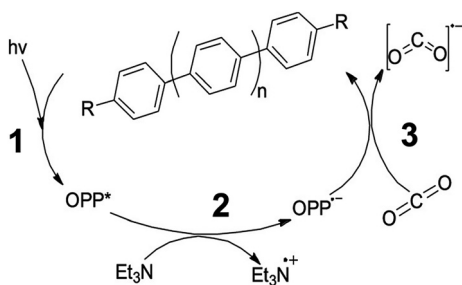


**Fig. 1:** Proposed catalytic cycle of single-electron reduction of CO<sub>2</sub> with oligo-*p*-phenylene (reproduced with permission from Ref. 32). Step 1 involves the photoexcitation of OPP-*n* to the first singlet excited state followed by reductive quenching by Et<sub>3</sub>N in step 2 to generate a radical anion that reduces CO<sub>2</sub> in step 3.

We computed the optimized structures of the molecules on the first singlet excited state ( $S_1$ ) in cyclohexane using TD-DFT ( $\omega$ B97X-D3/aug-cc-pVDZ) starting from the optimized ground-state structures. We then calculated the emission energies as the energy differences between  $S_1$  and  $S_0$  at the  $S_1$  optimized geometry. Solvent effects were described using the conductor-like polarizable continuum model (C-PCM).<sup>37</sup> We used the linear response approach to describe out-of-equilibrium solvent effects for vertical excitation and emission energies.<sup>38,39</sup> All transition energies were calculated with structures optimized in cyclohexane solvent. Exciton descriptors<sup>40–45</sup> were computed using *libwfa* library.<sup>42,46</sup> Natural transition orbitals (NTOs)<sup>44,47–49</sup> were visualized using IQmol molecular builder software with 0.1 isovalue.

Fluorescence lifetimes were calculated using

$$\tau_{fl} = \frac{2\pi \left(\frac{c}{n}\right)^3 \epsilon}{E_{em}^2 f_L}, \quad (1)$$

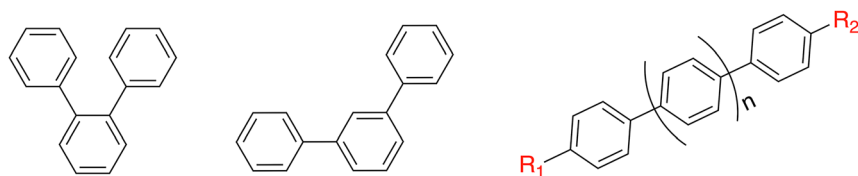
where we assumed atomic units,  $c$  is the velocity of light,  $n$  is the refractive index of the medium (1.4269 for cyclohexane at 20 °C),  $\epsilon$  is the dielectric constant of the medium (2.03 for cyclohexane at 20 °C),  $E_{em}$  is the emission energy and  $f_L$  is the oscillator strength.<sup>50</sup>

## Results and discussion

### Isomers of terphenyl

Terphenyl exists in three distinct isomeric forms – *ortho*-terphenyl (OOP-3), *meta*-terphenyl (OMP-3), and *para*-terphenyl (OPP-3). Figure 2 shows structures of these isomers. These structural differences result in markedly different photophysical properties, which in turn influence their applicability in photoredox catalysis. Table 1 presents the computed vertical excitation energies of the first three singlet excited states for each isomer. NTOs associated with the brightest electronic transition of the isomers are shown in Fig. 3. We observe that the vertical excitation energy ( $E^v$ ) increases and the oscillator strength decreases significantly for OOP-3 and OMP-3 relative to OPP-3. Lower oscillator strengths observed for the *ortho*- and *meta*-isomers are consistent with previous reports and result from reduced conjugation in these structures compared to the *para*-isomer.<sup>51</sup> The *meta*-isomer is cross-conjugated,<sup>52</sup> whereas in the *ortho*-isomer, conjugation is disrupted by steric repulsion. Notably, Table 1 shows that whereas the brightest transition in OPP-3 corresponds to the  $S_0 \rightarrow S_1$  excitation, the most intense transitions in OOP-3 and OMP-3 correspond to the excitation to high-lying singlet excited states. This is undesirable for photoredox catalysis because higher energy photons are needed to generate radical anions.<sup>53</sup>

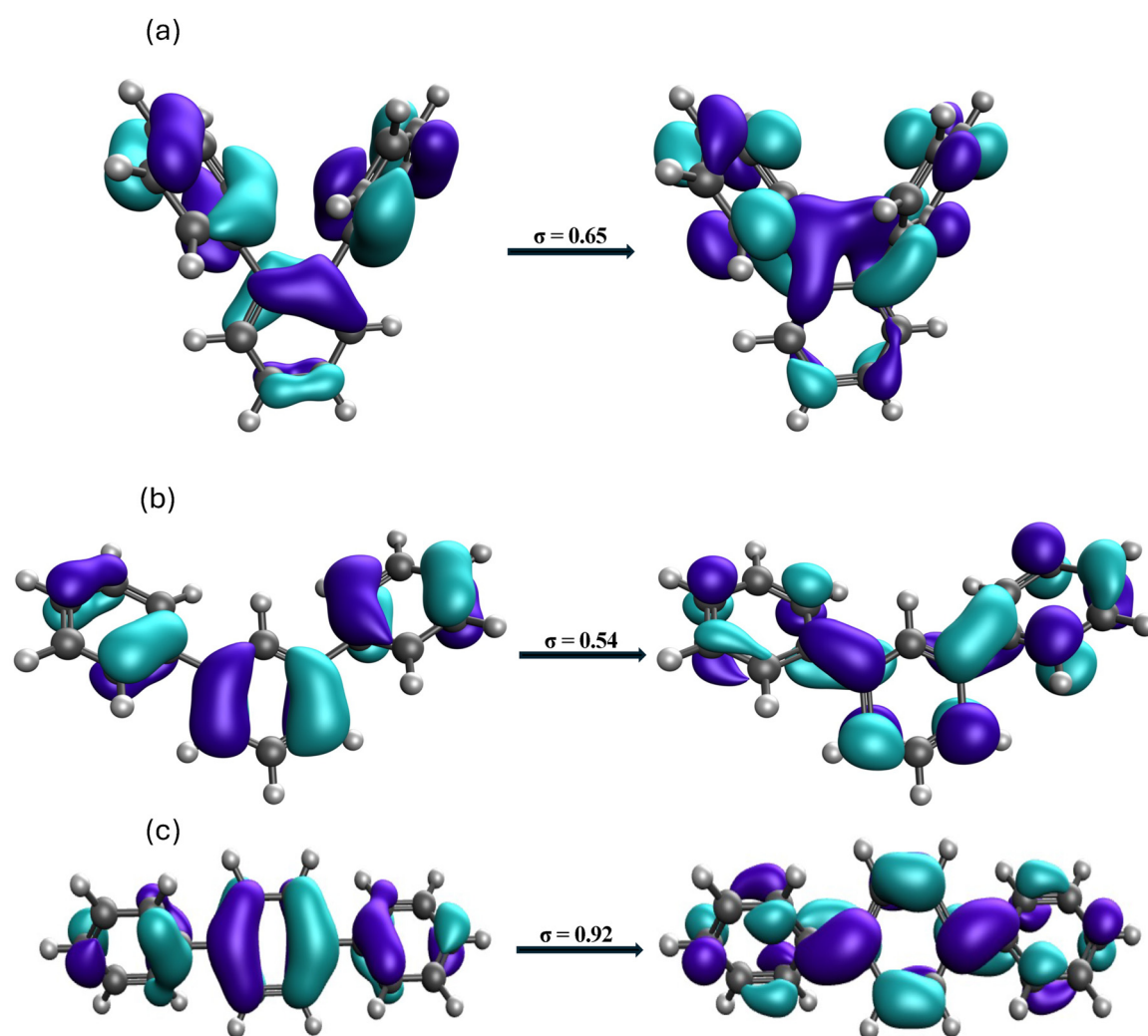
Table 2 shows the effects of solvent on the optical gap of the isomers. The nature of the brightest transition in cyclohexane is retained across solvents with higher optical dielectric constants and the shift in excitation energies is negligible. However, we observe a noticeable increase in oscillator strength for the brightest transitions of all isomers in more polar solvent environments. We also find a clear correlation between the optical dielectric constant of the solvent and the corresponding oscillator strength, with the latter increasing with solvent polarity.



**Fig. 2:** From left to right, *ortho*-terphenyl (OOP-3), *meta*-terphenyl (OMP-3), and *para*-terphenyl (OPP-3,  $n = 1$ ,  $R_1 = R_2 = H$ ).

**Table 1:** Vertical excitation energies ( $E^v$ , eV), of terphenyl isomers; oscillator strengths are given in parentheses.<sup>a</sup>

Isomer	$E^v(fl)$	State
OOP-3	5.11 (0.004)	$S_1$
	5.16 (0.122)	$S_2$
	5.30 (0.007)	$S_3$
OMP-3	5.00 (0.009)	$S_1$
	5.21 (0.131)	$S_2$
	5.32 (0.045)	$S_3$
OPP-3	4.88 (1.254)	$S_1$
	5.05 (0.000)	$S_2$
	5.20 (0.000)	$S_3$

<sup>a</sup>LRC- $\omega$ PBE/aug-cc-pVDZ.**Fig. 3:** Hole and particle NTOs and the corresponding singular values of (a) OOP-3, (b) OMP-3, and (c) OPP-3 in cyclohexane solvent; LRC- $\omega$ PBE/aug-cc-pVDZ, isovalue of 0.1.

**Table 2:** Vertical excitation energies (eV) of terphenyl isomers in cyclohexane; oscillator strengths are given in parentheses.<sup>a</sup>

Solvent	OPP-3 <sup>b</sup>	OMP-3 <sup>b</sup>	OPP-3
CyHEX	5.16 (0.12)	5.21 (0.13)	4.88 (1.25)
Bu <sub>2</sub> O	5.15 (0.17)	5.17 (0.32)	4.85 (1.36)
Et <sub>2</sub> O	5.14 (0.21)	5.14 (0.38)	4.82 (1.42)
PhBr	5.14 (0.21)	5.14 (0.39)	4.81 (1.45)
CH <sub>2</sub> Cl <sub>2</sub>	5.13 (0.26)	5.12 (0.43)	4.79 (1.51)

<sup>a</sup>LRC- $\omega$ PBE/aug-cc-pVDZ. <sup>b</sup>S<sub>2</sub> is the brightest state.

## Optical properties of oligo-*p*-phenylene

Table 3 shows the vertical excitation energies of the brightest transitions for the three *para*-oligomers – OPP-3 ( $n = 1$ ,  $R_1 = R_2 = H$ ), OPP-4 ( $n = 2$ ,  $R_1 = R_2 = H$ ), and OPP-5 ( $n = 3$ ,  $R_1 = R_2 = H$ ). In all species, the brightest transition corresponds to  $S_0 \rightarrow S_1$ . An intuitive interpretation based on Hückel's molecular orbital theory suggests that the optical gaps of oligo-*(p)*-phenylene systems are strongly influenced by the extent of delocalization, which is governed by the torsion angles between adjacent phenylene units. Planar structures exhibit maximal  $\pi$ -conjugation, whereas conjugation is disrupted for torsion angles approaching 90°. <sup>51</sup> Additionally, the excitation energy in OPP-3 can be tuned by increasing the number of phenylene units.

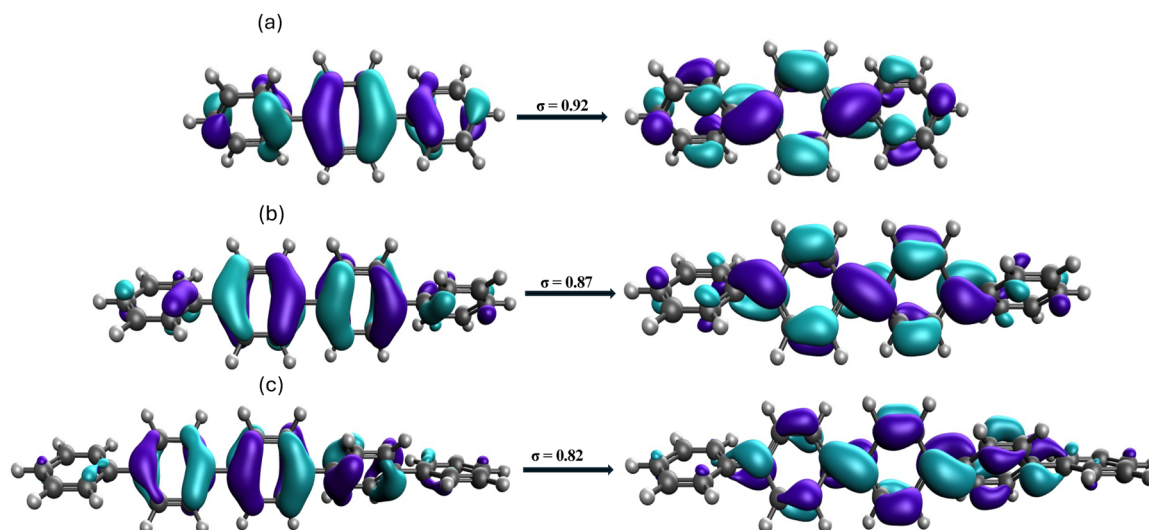
Among the oligomers examined, OPP-5 exhibits the highest degree of conjugation and, consequently, shows the lowest vertical excitation energies for the first singlet excited states. In contrast, OPP-3, with the shortest conjugation length, has the highest excitation energy. The observed red-shift in excitation energy with increasing oligomer size can be rationalized with a simple particle-in-a-box model, where the excitation energy is inversely proportional to the square of the molecule's effective conjugation length. However, the red-shift in excitation energies from OPP-3 to OPP-5 is not large (0.34 eV in cyclohexane), suggesting that the excitation energy is influenced not only by the conjugation length but also by the nature of the exciton. Lower excitation energies in higher oligomers are spectroscopically attractive but these oligomers are not effective for photo-reduction of CO<sub>2</sub> due to their high susceptibility to photobirch reduction in protic solvents. <sup>21</sup> OPP-5 also has low solubility.

Figure 4 shows NTOs for the  $S_0 \rightarrow S_1$  transition of the oligomers in cyclohexane. As expected, these transitions are characterized by delocalized  $\pi \rightarrow \pi^*$  excitations with no indication of charge-transfer character. This transition character remains unchanged across the other solvents examined in this study. As shown in Fig. 4, the hole NTOs reside on the phenylene units, whereas the electron NTOs reside over the bridging phenylene bonds. In OPP-4 and OPP-5, the exciton becomes increasingly localized toward the central phenylene units, which is consistent with the relatively small red-shift in absorption observed between OPP-3 and the longer-chain oligomers.

**Table 3:** Vertical excitation energies (eV) for  $S_0 \rightarrow S_1$  of oligo-*p*-phenylene; oscillator strengths are given in parentheses.<sup>a</sup>

Solvent	OPP-3	OPP-4	OPP-5
CyHEX	4.88 (1.25)	4.69 (1.84)	4.54 (2.43)
Bu <sub>2</sub> O	4.85 (1.36)	4.70 (1.79)	4.51 (2.53)
Et <sub>2</sub> O	4.82 (4.81)	4.64 (2.01)	4.53 (2.39)
PhBr	4.81 (1.45)	4.70 (1.80)	4.52 (2.39)
CH <sub>2</sub> Cl <sub>2</sub>	4.79 (1.51)	4.70 (1.80)	4.54 (2.39)

<sup>a</sup>LRC- $\omega$ PBE/aug-cc-pVDZ.



**Fig. 4:** Hole and particle NTOs and the corresponding singular values of (a) OPP-3, (b) OPP-4, and (c) OPP-5 in cyclohexane solvent; LRC- $\omega$ PBE/aug-cc-pVDZ, isovalue of 0.1.

## Absorption spectra of functionalized *p*-terphenyl

We examine the impact of terminal substitutions on the photophysical properties of OPP-3. Specifically, we study symmetric substitution with electron-donating ( $\text{NH}_2$ , OH) and electron-withdrawing (Br, F,  $\text{NO}_2$ , CN, Ac, Acac) substituents at the terminal phenylene units (see Table 4). The classification of substituents as electron-donating or withdrawing is based on the Hammett parameters reported by Hansch *et al.*<sup>54</sup> The effect of push-pull electronic structures introduced via asymmetric substitution on OPP-3 is summarized in Table 5.

Compared to the unsubstituted OPP-3, we observe a red-shift in excitation energy and a significant increase in the oscillator strength of the brightest transition for all symmetric derivatives except the fluoro derivative, which shows lower oscillator strength. The diacetylene substituent on the OPP-3 lowers the excitation energy the most (by 0.69 eV), whereas the fluoro substituent does it the least. In general, the brightest transition remains excitation from  $S_0$  to  $S_1$  and retains its  $\pi\pi^*$  character. For the  $\text{NO}_2$ -substituted *p*-terphenyl, the excitation to low-lying states ( $S_1$  and  $S_2$ ) involves the lone pair of electrons of  $\text{NO}_2$  and not the  $\pi$ -electrons on the phenylene units. The brightest transition for this system is from  $S_0$  to  $S_3$  and involves the  $\pi$  electrons of the terphenyl ring. The NTOs for nitro-substituted OPP-3 are shown in Fig. S1 in the SI. Similarly to the parent *p*-terphenyl, the derivatives also show a slight red-shift in excitation energies with increasing solvent polarity.

**Table 4:** Vertical excitation energies (eV) for  $S_0 \rightarrow S_1$  of symmetrically substituted *p*-terphenyl; oscillator strengths are given in parentheses.<sup>a</sup>

$R_1 = R_2$	CyHex	Bu <sub>2</sub> O	Et <sub>2</sub> O	PhBr	CH <sub>2</sub> Cl <sub>2</sub>
H	4.88 (1.25)	4.85 (1.36)	4.82 (1.42)	4.81 (1.45)	4.79 (1.51)
Br	4.84 (1.90)	4.66 (1.77)	4.64 (1.83)	4.63 (1.86)	4.62 (1.91)
F	4.85 (1.22)	4.82 (1.32)	4.80 (1.37)	4.79 (1.40)	4.77 (1.45)
$\text{NO}_2^b$	4.27 (1.57)	4.23 (1.65)	4.22 (1.70)	4.21 (1.72)	4.19 (1.77)
CN	4.65 (1.81)	4.48 (1.92)	4.46 (1.98)	4.45 (2.0)	4.43 (2.06)
Ac	4.46 (2.03)	4.42 (2.14)	4.40 (2.21)	4.39 (2.23)	4.37 (2.29)
Acac	4.16 (2.50)	4.13 (2.63)	4.11 (2.71)	4.10 (2.74)	4.09 (2.81)
$\text{NH}_2$	4.43 (1.60)	4.39 (1.71)	4.37 (1.77)	4.36 (1.80)	4.34 (1.86)
OH	4.19 (1.43)	4.14 (1.52)	4.12 (1.57)	4.11 (1.60)	4.19 (1.43)

<sup>a</sup>LRC- $\omega$ PBE/aug-cc-pVDZ; Ac, acetylene; Acac, diacetylene. <sup>b</sup> $S_3$  is the brightest state.

**Table 5:** Vertical excitation energies (eV) for  $S_0 \rightarrow S_1$  of asymmetrically substituted *p*-terphenyl; oscillator strengths are given in parentheses.<sup>a</sup>

$R_1$	$R_2$	CyHex	Bu <sub>2</sub> O	Et <sub>2</sub> O	PhBr	CH <sub>2</sub> Cl <sub>2</sub>
NO <sub>2</sub>	H <sup>b</sup>	4.26 (1.16)	4.22 (1.22)	4.20 (1.27)	4.20 (1.28)	4.18 (1.32)
NO <sub>2</sub>	NH <sub>2</sub> <sup>b</sup>	4.12 (1.27)	4.09 (1.24)	4.08 (1.14)	4.07 (1.08)	4.06 (0.88)
NO <sub>2</sub>	OH <sup>b</sup>	4.27 (1.21)	4.24 (1.28)	4.22 (1.31)	4.20 (1.33)	4.19 (1.36)
NO <sub>2</sub>	Br <sup>b</sup>	4.26 (1.29)	4.23 (1.36)	4.20 (1.41)	4.20 (1.41)	4.18 (1.44)
CN	NH <sub>2</sub>	4.37 (1.61)	4.33 (1.71)	4.31 (1.77)	4.30 (1.79)	4.28 (1.85)
CN	OH	4.51 (1.55)	4.48 (1.65)	4.46 (1.71)	4.45 (1.73)	4.43 (1.79)
Br	H	4.76 (1.46)	4.72 (1.57)	4.70 (1.64)	4.69 (1.65)	4.67 (1.71)
NH <sub>2</sub>	H	4.53 (1.36)	4.49 (1.45)	4.46 (1.53)	4.46 (1.53)	4.43 (1.59)
NH <sub>2</sub>	Br	4.51 (1.54)	4.47 (1.64)	4.45 (1.71)	4.44 (1.72)	4.42 (1.77)
NH <sub>2</sub>	F	4.60 (1.31)	4.59 (1.31)	4.60 (1.31)	4.59 (1.31)	4.59 (1.31)
OH	F	4.76 (1.25)	4.76 (1.25)	4.76(1.25)	4.76(1.25)	4.77(1.25)

<sup>a</sup>LRC- $\omega$ PBE/aug-cc-pVDZ. <sup>b</sup> $S_2$  is the brightest state.

Asymmetric substitution to OPP-3 ( $R_1 \neq R_2$ ) also results in a red-shift in absorption relative to the parent molecule. Among the substituents studied, the push-pull system incorporating NO<sub>2</sub> and NH<sub>2</sub> groups induces the most significant red-shift. In the push-pull OPP-3 with a single NO<sub>2</sub> substituent, only the transition to the  $S_1$  state involves non-bonding electrons on the NO<sub>2</sub> group, whereas the brightest transition corresponds to excitation to the  $S_2$  state and involves the  $\pi$ -electron of the phenylene units. Figure 5 shows the NTOs of selected push-pull derivatives of OPP-3.

Table S1 in the SI summarizes the effect of substituents on the absorption spectra of OPP-4 and OPP-5. Similar to OPP-3, the derivatives of OPP-4 and OPP-5 exhibit brighter transitions and lower excitation energies than their parent molecules. In particular, the nitro-substituted OPP-4 and OPP-5 show nearly identical  $S_1$  and  $S_2$  transitions with the same excitation energies, indicating that these transitions are independent of the chain length. However, unlike in OPP-3, the NO<sub>2</sub> and NH<sub>2</sub> push-pull substitution does not lead to the notable red-shift in absorption. This behavior is discussed in detail in the exciton analysis section, where we show that the effect of substituents on excitation energy depends on the exciton size.

## Exciton analysis

We compare the exciton properties of the parent catalyst with its derivatives for the brightest transition from the ground state. Fig. 6 shows the exciton size and correlation coefficient for the brightest transition of the parent

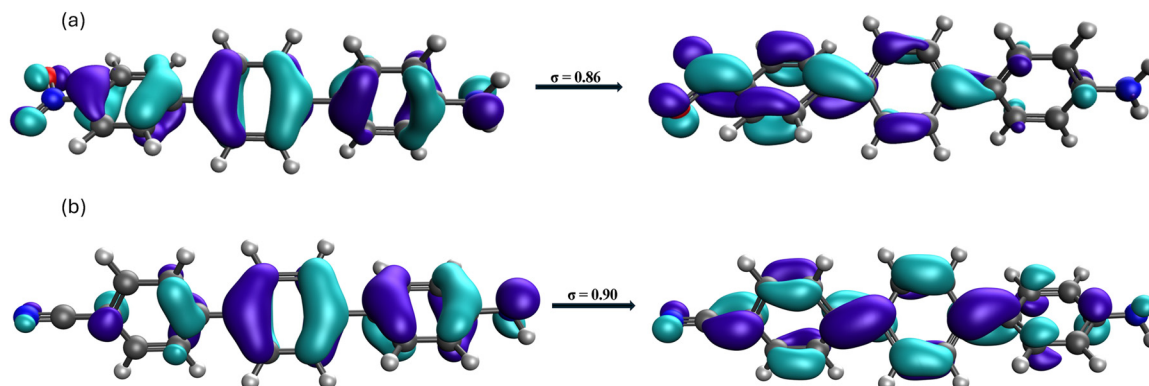


**Fig. 5:** Hole and particle NTOs and the corresponding singular values for the brightest transition for push-pull derivatives of OPP-3; (a) OPP-3 ( $R_1 = \text{NO}_2$ ,  $R_2 = \text{NH}_2$ ) and (b) OPP-3 ( $R_1 = \text{CN}$ ,  $R_2 = \text{NH}_2$ ) in cyclohexane solvent; LRC- $\omega$ PBE/aug-cc-pVDZ, isovalue of 0.1.

OPP-3 and its derivatives. Table 6 presents additional exciton descriptors for OPP-3. These quantities provide insight into the nature of various excited states. The exciton size quantifies the charge-resonance character whereas the electron–hole distance captures the extent of permanent charge-transfer character in the molecule. The correlation coefficient measures the spatial correlation of electron and hole positions in molecules.<sup>36,40,44–46</sup>

We observe a slight increase in exciton size in most OPP-3 derivatives, with the largest increase found in push–pull systems. The derivatives exhibit more strongly bound exciton pairs (higher correlation coefficient) than the parent molecule. Table 6 shows that the average electron–hole distance ( $d_{h \rightarrow e}$ ) is zero for all symmetric derivatives, indicating valence excitations where both the hole and electron NTOs reside on the same fragments in the molecule. However, asymmetrically substituted OPP-3 derivatives show significantly higher values of  $d_{h \rightarrow e}$ . Once again, push–pull systems exhibit the greatest electron–hole separation, consistent with their NTOs. The hole NTOs in these derivatives are more localized on the phenylene unit bearing the electron-donating group while the electron NTOs are shifted toward the electron-withdrawing substituent. As a result, these derivatives acquire a charge transfer character. This acquired charge-transfer character is more pronounced in the  $\text{NO}_2$ - and  $\text{NH}_2$ -substituted system.

Symmetric and asymmetric substituents on OPP-3 induce minimal changes to the ground-state structure but they significantly redshift excitation energy. This indicates that the substituents alter the nature of the exciton. As shown in Fig. 6, all substituents exhibit larger exciton size than the parent OPP-3, with push-pull derivatives showing the largest increases. Notably,  $\text{NO}_2$  and  $\text{NH}_2$  derivative show the largest exciton sizes and the lowest excitation energies among all derivatives. In contrast, the fluoro-substituted derivative shows no change in exciton size, in line with the observed minimal reduction in the excitation energy.

Figure 7 compares the exciton size and correlation coefficient of the longer-chain oligomers and their derivatives. We observe a slight increase in exciton size with increasing oligomer length. The intrinsic Coulomb attraction between the hole and electron limits further delocalization in longer-chain oligomers. However, the exciton remains more strongly bound in the longer-chain oligomers. The influence of the  $\text{NO}_2$  and  $\text{NH}_2$  push–pull effect on the exciton size is more pronounced in OPP-3 than in OPP-4 or OPP-5. The  $\text{NO}_2$  and  $\text{NH}_2$  derivative shows the lowest excitation energy in OPP-3 than in other oligomers. Across all species studied, we observed that the excitation energy decreases with increasing exciton size.

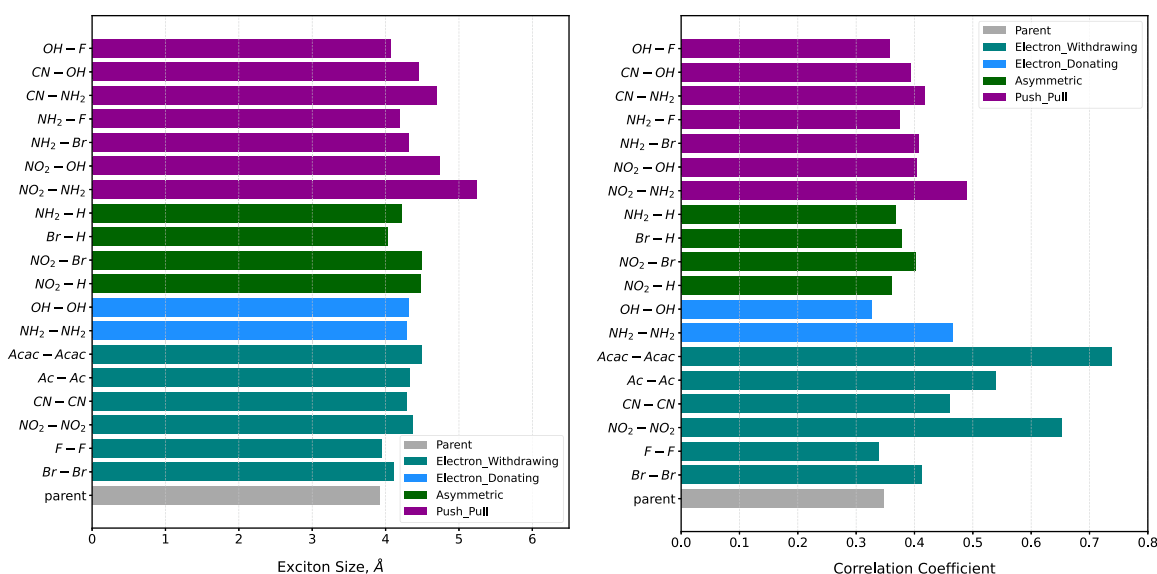


**Fig. 6:** Exciton size (left) and correlation coefficient (right) of functionalized OPP-3 in cyclohexane solvent; LRC- $\omega$ PBE/aug-cc-pVDZ. The correlation coefficient is dimensionless.

**Table 6:** Hole size ( $\sigma_h$ ), electron size ( $\sigma_e$ ), and electron-hole distance ( $d_{h \rightarrow e}$ ) of functionalized *p*-terphenyl.<sup>a</sup>

$R_1$	$R_2$	$\sigma_h$ (Å)	$\sigma_e$ (Å)	$d_{h \rightarrow e}$ (Å)
H	H	3.429	3.529	0.000
Br	Br	3.795	3.775	0.000
F	F	3.441	3.421	0.000
NO <sub>2</sub>	NO <sub>2</sub> <sup>b</sup>	4.155	5.741	0.003
CN	CN	3.784	4.399	0.000
Ac	Ac	4.428	4.596	0.000
Acac	Acac	6.089	6.307	0.002
NH <sub>2</sub>	NH <sub>2</sub>	4.409	3.828	0.008
OH	OH	3.855	3.556	0.000
NO <sub>2</sub>	H	3.384	3.597	2.120
NO <sub>2</sub>	NH <sub>2</sub>	4.611	4.317	2.655
NO <sub>2</sub>	OH	3.750	3.771	2.350
NO <sub>2</sub>	Br	3.528	3.801	2.020
CN	NH <sub>2</sub>	4.001	4.071	1.740
CN	OH	3.820	3.876	1.372
Br	H	3.588	3.628	0.070
NH <sub>2</sub>	H	3.653	3.611	1.064
NH <sub>2</sub>	Br	3.899	3.762	1.114

<sup>a</sup>LRC- $\omega$ PBE/aug-cc-pVDZ. <sup>b</sup>S<sub>3</sub> is the brightest state.

## Excited states and fluorescence behavior of oligo-*p*-phenylenes

Figure 8 shows the optimized S<sub>1</sub> structure of oligomers and selected derivatives. The torsion angle between carbon atoms on adjacent phenylene units is shown. The inter-phenylene carbon-carbon bond distance is also given. OPP-3 is twisted in the ground state, but is planar in S<sub>1</sub>. This planarization in the excited state facilitates the generation of the radical anion via interaction with a sacrificial electron donor during CO<sub>2</sub> photoreduction. The derivatives of OPP-3 exhibit similar structural behavior in their ground and S<sub>1</sub> excited states, with torsion angles between adjacent phenylene units deviating slightly from 0°. An exception is the nitro-substituted terphenyl, which adopts a twisted geometry in its relaxed S<sub>1</sub> state – consistent with the nature of its electronic excitation to S<sub>1</sub>. OPP-4 and OPP-5 retain their twisted geometries in the excited state; however, the inner phenylene units become planar while the terminal units are not in plane.

Tables 7 and 8 show the emission energies of [OPP-3]\* and its derivatives. Whereas absorption spectra consistently show red-shifted excitation energies for all derivatives, the corresponding emission energies exhibit no systematic trend relative to the parent molecule. The diacetylene derivative of OPP-3 displays the most red-shifted emission among all symmetric substitutions, whereas the nitro-substituted OPP-3 shows the most blue-shifted emission relative to the parent catalyst. Similar to the parent [OPP-3]\*, the derivatives display minimal solvatochromic shifts in their emission energies. However, their radiative transition strengths increase with solvent polarity, which is consistent with the behavior of the parent chromophore. Among the derivatives, asymmetric substitutions induce the largest shifts in fluorescence energy. Notably, the NO<sub>2</sub>- and NH<sub>2</sub>-substituted push-pull system displays the largest red-shift in emission energy relative to the parent, with a shift of 0.88 eV. As with the symmetric derivatives, the asymmetric variants also show solvatochromic shifts similar in magnitude to those of the parent.

Figure 9 presents the computed intrinsic fluorescence lifetimes of various derivatives, normalized to that of the parent [OPP-3]\*. Consistent with Eqn. (1), brighter emission – such as that observed for the diacetylene derivative of OPP-3 – is associated with shorter fluorescence lifetimes. Nearly all push-pull derivatives (except CN and OH derivative) show longer fluorescence lifetime relative to the parent, with NO<sub>2</sub> and NH<sub>2</sub> derivative exhibiting the longest lifetime. Extended fluorescence lifetimes can be beneficial for generating the reducing radical anion, as they provide more time for the sacrificial molecule and [OPP-3]\* to interact. However, longer

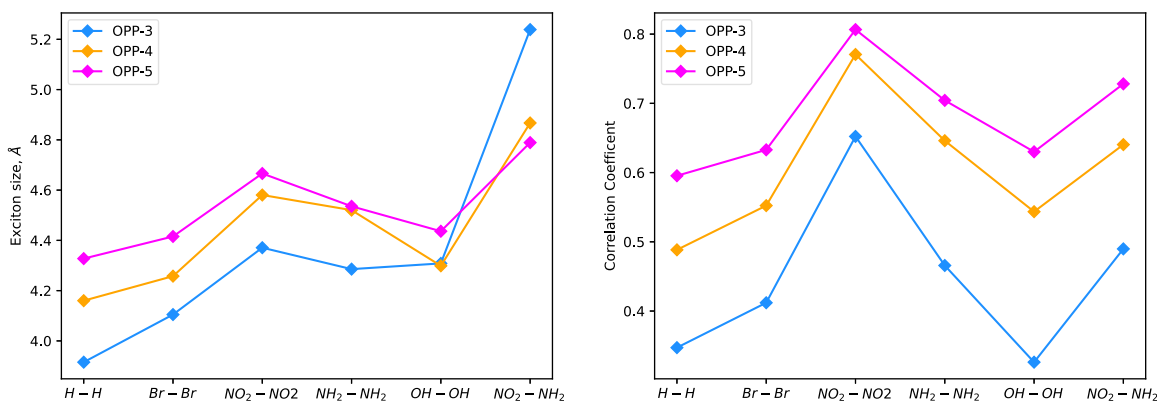


**Fig. 7:** Exciton size (left) and correlation coefficient (right) of functionalized oligomers in cyclohexane solvent; LRC- $\omega$ PBE/aug-cc-pVDZ. The correlation coefficient is dimensionless.

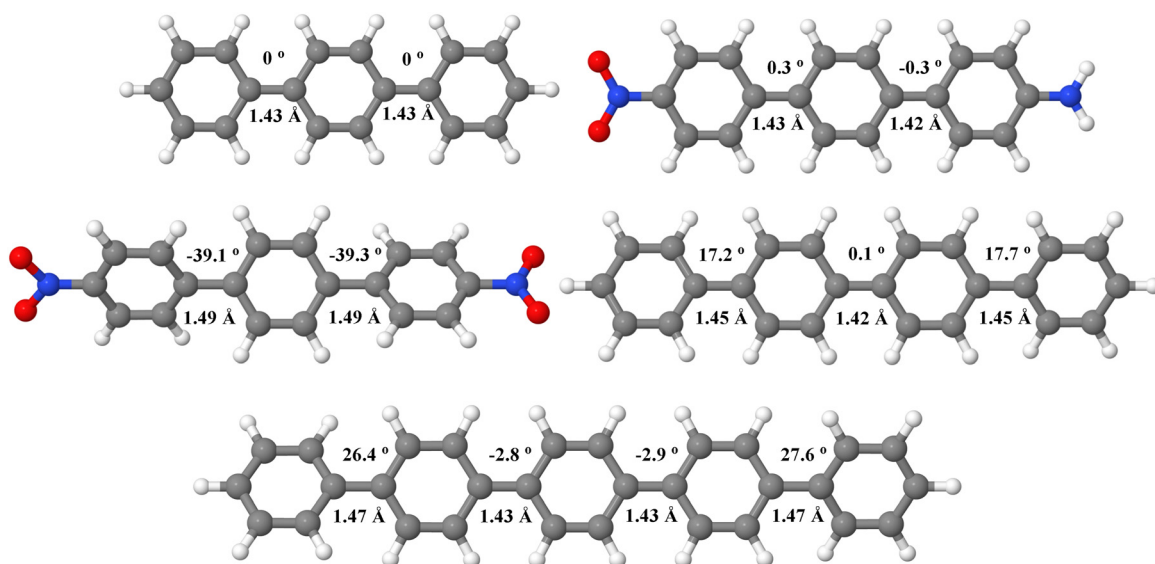


**Fig. 8:** S<sub>1</sub> optimized structure of molecules. From top left; [OPP-3]\*, [OPP-3]\* (R<sub>1</sub> = NO<sub>2</sub>, R<sub>2</sub> = NH<sub>2</sub>), [OPP-3]\* (R<sub>1</sub> = R<sub>2</sub> = NO<sub>2</sub>), [OPP-4]\* and [OPP-5]\*. Dihedral angles between carbon atoms on adjacent phenylene units and the C-C bond lengths connecting phenylene units are shown.

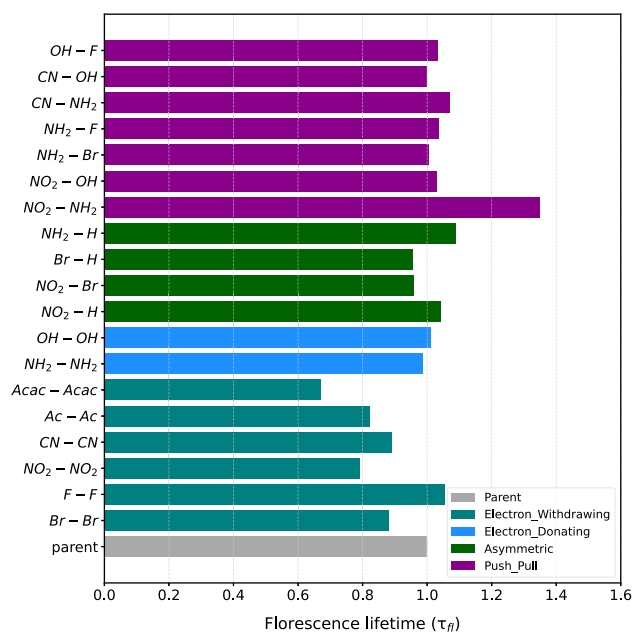
**Table 7:** Emission energies (eV) of symmetrically substituted *p*-terphenyl; oscillator strengths are given in parentheses.<sup>a</sup>

R <sub>1</sub> = R <sub>2</sub>	CyHex	Bu <sub>2</sub> O	Et <sub>2</sub> O	PhBr	CH <sub>2</sub> Cl <sub>2</sub>
H	3.62 (1.36)	3.56 (1.44)	3.53 (1.49)	3.52 (1.51)	3.49 (1.56)
Br	3.45 (1.70)	3.40 (1.78)	3.37 (1.82)	3.36 (1.84)	3.33 (1.88)
F	3.55 (1.34)	3.50 (1.42)	3.47 (1.46)	3.46 (1.48)	3.43 (1.52)
NO <sub>2</sub>	3.76 (1.59)	3.82 (1.50)	3.78 (1.56)	3.78 (1.56)	3.76 (1.59)
CN	3.36 (1.77)	3.36 (1.78)	3.36 (1.78)	3.36 (1.79)	3.36 (1.79)
Ac	3.30 (1.99)	3.25 (2.07)	3.21 (2.12)	3.20 (2.14)	3.18 (2.19)
Acac	3.17 (2.64)	3.13 (2.73)	3.10 (2.77)	3.09 (2.79)	3.07 (2.83)
NH <sub>2</sub>	3.27 (1.69)	3.22 (1.79)	3.18 (1.84)	3.17 (1.86)	3.14 (1.91)
OH	3.44 (1.49)	3.39 (1.57)	3.36 (1.62)	3.34 (1.64)	3.31 (1.68)

<sup>a</sup>LRC- $\omega$ PBE/aug-cc-pVDZ.

**Table 8:** Emission energies (eV) of asymmetrically substituted *p*-terphenyl; oscillator strengths are given in parentheses.<sup>a</sup>

$R_1$	$R_2$	CyHex	Bu <sub>2</sub> O	Et <sub>2</sub> O	PhBr	CH <sub>2</sub> Cl <sub>2</sub>
NO <sub>2</sub>	H	3.84 (1.16)	3.80 (1.22)	3.77 (1.26)	3.76 (1.27)	3.73 (1.30)
NO <sub>2</sub>	NH <sub>2</sub>	2.74 (1.76)	2.67 (1.85)	2.63 (1.91)	2.62 (1.92)	2.59 (1.96)
NO <sub>2</sub>	OH	3.78 (1.21)	3.73 (1.27)	3.70 (1.32)	3.69 (1.32)	3.67 (1.35)
NO <sub>2</sub>	Br	3.89 (1.23)	3.84 (1.28)	3.81 (1.31)	3.80 (1.32)	3.78 (1.34)
CN	NH <sub>2</sub>	2.90 (1.98)	2.99 (1.86)	2.95 (1.91)	2.93 (1.93)	2.90 (1.98)
CN	OH	3.27 (1.67)	3.21 (1.76)	3.18 (1.80)	3.17 (1.82)	3.14 (1.87)
Br	H	3.49 (1.53)	3.44 (1.61)	3.40 (1.67)	3.40 (1.68)	3.37 (1.72)
NH <sub>2</sub>	H	3.28 (1.52)	3.22 (1.61)	3.18 (1.67)	3.17 (1.68)	3.14 (1.72)
NH <sub>2</sub>	Br	3.23 (1.70)	3.17 (1.75)	3.13 (1.81)	3.12 (1.82)	3.09 (1.86)
NH <sub>2</sub>	F	3.43 (1.46)	3.43 (1.46)	3.43 (1.46)	3.43 (1.46)	3.42 (1.46)
OH	F	3.55 (1.37)	3.56 (1.37)	3.56 (1.37)	3.56 (1.37)	3.56 (1.38)

<sup>a</sup>LRC-*w*PBE/aug-cc-pVDZ.**Fig. 9:** Fluorescence lifetimes of derivatives normalized to the parent OPP-3 in cyclohexane solvent; LRC-*w*PBE/aug-cc-pVDZ.

lifetimes can also result in other undesirable relaxation channels, such as radiative relaxation to the ground state.

## Conclusions

We examine the photophysical properties of substituted oligophenylenes and identify those with traits that are desirable in photoredox catalysts for reactions including for CO<sub>2</sub> reduction and hydrogen evolution. The main findings can be summarized as follows:

- (1) The excitation of OPP-*n* is dominated by a transition between delocalized  $\pi$  and  $\pi^*$  orbitals (corresponding to the HOMO-LUMO transition). In the parent oligo-*p*-phenylene, the excitation is delocalized and exhibits  $\pi \rightarrow \pi^*$  character. Similarly to OPP-*n*, the brightest transitions in *ortho*- and *meta*-terphenyls are also primarily of HOMO-LUMO character.
- (2) The absorption energy of OPP-*n* can be lowered through terminal substitution. The oscillator strength of the brightest transition increases significantly for all substituted derivatives, allowing easier generation of the

radical anion for catalysis through increased excited-state population. Push–pull substituents induce a notable red-shift in absorption energies, and all derivatives studied display solvatochromic shifts similar to those of the parent chromophores.

- (3) The increase in the exciton size from [OPP-3]\* to [OPP-5]\* is small. Coulomb attraction between the hole and electron limits further delocalization in higher oligomers. The exciton in both OPP-*n* and their derivatives is localized and shows a positive spatial correlation between the hole and electron. In contrast, push–pull derivatives acquire charge-transfer character.
- (4) Terminal substitution has a negligible effect on the planarization of OPP-3 in the excited state – a key factor facilitating interaction with sacrificial donor molecules. Additionally, the derivatives of OPP-3 exhibit longer fluorescence lifetimes.

Overall, our findings demonstrate that substituted OPP-*n* chromophores exhibit more favorable optical properties compared to the parent catalyst. Among the derivatives studied, push–pull chromophores emerge as optimal candidates for photoredox catalysis, striking a balance between lower absorption energy and prolonged fluorescence lifetimes – both key for efficient radical anion generation. Nonetheless, given the complexity of the photocatalytic process, further investigation of the subsequent electron-transfer steps is needed to fully assess the catalytic potential of these derivatives.

**Acknowledgments:** The authors acknowledge computational resources and support from USC's Center for Advanced Research Computing (CARC) and the National Energy Research Scientific Computing Center (NERSC).

**Research ethics:** Not applicable.

**Informed consent:** Not applicable.

**Author contributions:** All authors have accepted responsibility for the entire content of this manuscript and approved its submission.

**Use of Large Language Models, AI and Machine Learning Tools:** None declared.

**Conflict of interest:** The authors declare the following competing financial interest(s): A.I.K. is the president and a part-owner of Q-Chem, Inc.

**Research funding:** This work is supported by the U.S. Department of Energy, Office of Science, Office of Basic Energy Sciences under Award Numbers DE-SC0022326.

**Data availability:** The data supporting this study's findings are available within the article and its Supporting Information (SI) file. The relevant geometries are available in the SI.

## References

1. Davis, S. J.; Caldeira, K.; Matthews, H. D. Future CO<sub>2</sub> Emissions and Climate Change from Existing Energy Infrastructure. *Science* **2010**, *329*, 1330; <https://doi.org/10.1126/science.1188566>.
2. Ramanathan, V.; Feng, Y. On Avoiding Dangerous Anthropogenic Interference with the Climate System: Formidable Challenges Ahead. *Proc. Nat. Acad. Sci.* **2008**, *105*, 14245; <https://doi.org/10.1073/pnas.0803838105>.
3. Wigley, T. M. L. The Climate Change Commitment. *Science* **2005**, *307*, 1766; <https://doi.org/10.1126/science.1103934>.
4. Ha-Duong, M.; Grubb, M. J.; Hourcade, J. C. Influence of Socioeconomic Inertia and Uncertainty on Optimal CO<sub>2</sub>-Emission Abatement. *Nature* **1997**, *390*, 270; <https://doi.org/10.1038/36825>.
5. Matthews, H. D.; Wynes, S. Current Global Efforts Are Insufficient to Limit Warming to 1.5 C. *Science* **2022**, *376*, 1404; <https://doi.org/10.1126/science.abo3378>.
6. Yoro, K. O.; Daramola, M. O. CO<sub>2</sub> Emission Sources, Greenhouse Gases, and the Global Warming Effect. In *Advances in carbon capture*; Elsevier: Amsterdam, The Netherlands, 2020; pp 3–28.
7. Sahara, G.; Ishitani, O. Efficient Photocatalysts for CO<sub>2</sub> Reduction. *Inorg. Chem.* **2015**, *54*, 5096; <https://doi.org/10.1021/ic502675a>.
8. Fang, S.; Rahaman, M.; Bharti, J.; Reisner, E.; Robert, M.; Ozin, G. A.; Hu, Y. H. Photocatalytic CO<sub>2</sub> Reduction. *Nat. Rev. Methods Primers* **2023**, *3*, 61; <https://doi.org/10.1038/s43586-023-00243-w>.
9. Fu, J.; Jiang, K.; Qiu, X.; Yu, J.; Liu, M. Product Selectivity of Photocatalytic CO<sub>2</sub> Reduction Reactions. *Mater. Today* **2020**, *32*, 222; <https://doi.org/10.1016/j.mattod.2019.06.009>.
10. Albero, J.; Peng, Y.; García, H. Photocatalytic CO<sub>2</sub> Reduction to C<sub>2</sub><sup>+</sup> Products. *ACS Cat.* **2020**, *10*, 5734.

11. Kumagai, H.; Tamaki, Y.; Ishitani, O. Photocatalytic Systems for CO<sub>2</sub> Reduction: Metal-Complex Photocatalysts and Their Hybrids with Photofunctional Solid Materials. *Acc. Chem. Res.* **2022**, *55*, 978; <https://doi.org/10.1021/acs.accounts.1c00705>.
12. Windle, C. D.; Perutz, R. N. Advances in Molecular Photocatalytic and Electrocatalytic CO<sub>2</sub> Reduction. *Coord. Chem. Rev.* **2012**, *256*, 2562; <https://doi.org/10.1016/j.ccr.2012.03.010>.
13. Corma, A.; Garcia, H. Photocatalytic Reduction of CO<sub>2</sub> for Fuel Production: Possibilities and Challenges. *J. Catal.* **2013**, *308*, 168; <https://doi.org/10.1016/j.jcat.2013.06.008>.
14. Shi, R.; Waterhouse, G. I. N.; Zhang, T. Recent Progress in Photocatalytic CO<sub>2</sub> Reduction over Perovskite Oxides. *Solar Rrl* **2017**, *1*, 1700126; <https://doi.org/10.1002/solr.201700126>.
15. Zhang, X.; Wang, Y.; Gu, M.; Wang, M.; Zhang, Z.; Pan, W.; Jiang, Z.; Zheng, H.; Lucero, M.; Wang, H.; Sterbinsky, G. E.; Ma, Q.; Wang, Y. G.; Feng, Z.; Li, J.; Dai, H.; Liang, Y. Molecular Engineering of Dispersed Nickel Phthalocyanines on Carbon Nanotubes for Selective CO<sub>2</sub> Reduction. *Nat. Energy* **2020**, *5*, 684; <https://doi.org/10.1038/s41560-020-0667-9>.
16. Zhang, S.; Fan, Q.; Xia, R.; Meyer, T. J. CO<sub>2</sub> Reduction: From Homogeneous to Heterogeneous Electrocatalysis. *Acc. Chem. Res.* **2020**, *53*, 255; <https://doi.org/10.1021/acs.accounts.9b00496>.
17. Gao, J.; Shiong, S.; Choo, S.; Liu, Y. Reduction of CO<sub>2</sub> to Chemicals and Fuels: Thermocatalysis versus Electrocatalysis. *J. Chem. Eng.* **2023**, *472*, 145033.
18. Yaashikaa, P. R.; Kumar, P.; Senthil; Varjani, S. J.; Saravanan, A. A Review on Photochemical, Biochemical and Electrochemical Transformation of CO<sub>2</sub> into Value-Added Products. *J. CO<sub>2</sub> Utilization* **2019**, *33*, 131.
19. Matsuoka, S.; Kohzuki, T.; Pac, C.; Yanagida, S. Photochemical Reduction of Carbon Dioxide to Formate Catalyzed by P-Terphenyl in Aprotic Polar Solvent. *Chem. Lett.* **1990**, *19*, 2047; <https://doi.org/10.1246/cl.1990.2047>.
20. Matsuoka, S.; Fujii, H.; Yamada, T.; Pac, C.; Ishida, A.; Takamuku, S.; Kusaba, M.; Nakashima, N.; Yanagida, S. Photocatalysis of Oligo (P-phenylenes): Photoreductive Production of Hydrogen and Ethanol in Aqueous Triethylamine. *J. Phys. Chem.* **1991**, *95*, 5802; <https://doi.org/10.1021/j100168a018>.
21. Matsuoka, S.; Kohzuki, T.; Pac, C.; Ishida, A.; Takamuku, S.; Kusaba, M.; Nakashima, N.; Yanagida, S. Photocatalysis of Oligo (P-phenylenes): Photochemical Reduction of Carbon Dioxide with Triethylamine. *J. Phys. Chem.* **1992**, *96*, 4437; <https://doi.org/10.1021/j100190a057>.
22. Pipim, B.; Sampson, K.; Torres, J.; Tingey, N.; Flynn, K.; Depew, D.; Wang, J.; Krylov, A. Ab initio Simulations of Dynamics of EMI-BF<sub>4</sub> Ionic Liquid Propellant Used in Electrospray Thrusters for Nanosatellite Applications. *ChemRxiv* **2025**, <https://doi.org/10.26434/chemrxiv-2025-wsw0l-v2>.
23. Romero, N. A.; Nicewicz, D. A. Organic Photoredox Catalysis. *Chem. Rev.* **2016**, *116*, 10075; <https://doi.org/10.1021/acs.chemrev.6b00057>.
24. Shaw, M. H.; Twilton, J.; MacMillan, D. W. C. Photoredox Catalysis in Organic Chemistry. *J. Org. Chem.* **2016**, *81*, 6898; <https://doi.org/10.1021/acs.joc.6b01449>.
25. Hernandez-Perez, A. C.; Collins, S. K. Heteroleptic Cu-Based Sensitizers in Photoredox Catalysis. *Acc. Chem. Res.* **2016**, *49*, 1557; <https://doi.org/10.1021/acs.accounts.6b00250>.
26. Chen, R.; Hu, X. Q.; Lu, L. Q.; Xiao, W. J. Exploration of Visible-Light Photocatalysis in Heterocycle Synthesis and Functionalization: Reaction Design and beyond. *Acc. Chem. Res.* **2016**, *49*, 1911; <https://doi.org/10.1021/acs.accounts.6b00254>.
27. Jamison, C. R.; Overman, L. E. Fragment Coupling with Tertiary Radicals Generated by Visible-Light Photocatalysis. *Acc. Chem. Res.* **2016**, *49*, 1578; <https://doi.org/10.1021/acs.accounts.6b00284>.
28. Nakajima, K.; Miyake, Y.; Nishibayashi, Y. Synthetic Utilization of  $\alpha$ -aminoalkyl Radicals and Related Species in Visible Light Photoredox Catalysis. *Acc. Chem. Res.* **2016**, *49*, 1946; <https://doi.org/10.1021/acs.accounts.6b00251>.
29. Reiser, O. Shining Light on Copper: Unique Opportunities for Visible-Light-Catalyzed Atom Transfer Radical Addition Reactions and Related Processes. *Acc. Chem. Res.* **2016**, *49*, 1990; <https://doi.org/10.1021/acs.accounts.6b00296>.
30. Majek, M.; Jacobi von Wangelin, A. Mechanistic Perspectives on Organic Photoredox Catalysis for Aromatic Substitutions. *Acc. Chem. Res.* **2016**, *49*, 2316; <https://doi.org/10.1021/acs.accounts.6b00293>.
31. Kron, K. J.; Rodriguez-Katakura, A.; Elhessen, R.; Mallikarjun Sharada, S. Photoredox Chemistry with Organic Catalysts: Role of Computational Methods. *ACS Omega* **2021**, *6*, 33253; <https://doi.org/10.1021/acsomega.1c05787>.
32. Kron, K. J.; Gomez, S. J.; Mao, Y.; Cave, R. J.; Mallikarjun Sharada, S. Computational Analysis of Electron Transfer Kinetics for CO<sub>2</sub> Reduction with Organic Photoredox Catalysts. *J. Phys. Chem. A* **2020**, *124*, 5359; <https://doi.org/10.1021/acs.jpca.0c03065>.
33. Epifanovsky, E.; Gilbert, A. T. B.; Feng, X.; Lee, J.; Mao, Y.; Mardirossian, N.; Pokhilko, P.; White, A. F.; Coons, M. P.; Dempwolff, A. L.; Gan, Z.; Hait, D.; Horn, P. R.; Jacobson, L. D.; Kaliman, I.; Kussmann, J.; Lange, A. W.; Lao, K. U.; Levine, D. S.; Liu, J.; McKenzie, S. C.; Morrison, A. F.; Nanda, K. D.; Plasser, F.; Rehn, D. R.; Vidal, M. L.; You, Z.-Q.; Zhu, Y.; Alam, B.; Albrecht, B. J.; Aldossary, A.; Alguire, E.; Andersen, J. H.; Athavale, V.; Barton, D.; Begam, K.; Behn, A.; Bellonzi, N.; Bernard, Y. A.; Berquist, E. J.; Burton, H. G. A.; Carreras, A.; Carter-Fenk, K.; Chakraborty, R.; Chien, A. D.; Closser, K. D.; Cofer-Shabica, V.; Dasgupta, S.; de Wergifosse, M.; Deng, J.; Diedenhofen, M.; Do, H.; Ehlert, S.; Fang, P.-T.; Fatehi, S.; Feng, Q.; Friedhoff, T.; Gayvert, J.; Ge, Q.; Gidofalvi, G.; Goldey, M.; Gomes, J.; González-Espinoza, C. E.; Gulania, S.; Gunina, A. O.; Hanson-Heine, M. W. D.; Harbach, P. H. P.; Hauser, A.; Herbst, M. F.; Hernández Vera, M.; Hodecker, M.; Holden, Z. C.; Houck, S.; Huang, X.; Hui, K.; Huynh, B. C.; Ivanov, M.; Jász, Á.; Ji, H.; Jiang, H.; Kaduk, B.; Kähler, S.; Khistyayev, K.; Kim, J.; Kis, G.; Klunzinger, P.; Koczor-Benda, Z.; Koh, J. H.; Kosenkov, D.; Koulias, L.; Kowalczyk, T.; Krauter, C. M.; Kue, K.; Kunitsa, A.; Kus, T.; Ladžánszki, I.; Landau, A.; Lawler, K. V.; Lefrançois, D.; Lehtola, S.; Li, R. R.; Li, Y.-P.; Liang, J.; Liebenthal, M.; Lin, H.-H.; Lin, Y.-S.; Liu, F.; Liu, K.-Y.; Loipersberger, M.; Luenser, A.; Manjanath, A.; Manohar, P.; Mansoor, E.; Manzer, S. F.; Mao, S.-P.; Marenich, A. V.; Markovich, T.; Mason, S.; Maurer, S. A.; McLaughlin, P. F.; Menger, M. F. S. J.; Mewes, J.-M.; Mewes, S. A.; Morgante, P.; Mullinax, J. W.; Oosterbaan, K. J.;

- Paran, G.; Paul, A. C.; Paul, S. K.; Pavošević, F.; Pei, Z.; Prager, S.; Proynov, E. I.; Rák, Á.; Ramos-Cordoba, E.; Rana, B.; Rask, A. E.; Rettig, A.; Richard, R. M.; Rob, F.; Rossomme, E.; Scheele, T.; Scheurer, M.; Schneider, M.; Sergueev, N.; Sharada, S. M.; Skomorowski, W.; Small, D. W.; Stein, C. J.; Su, Y.-C.; Sundstrom, E. J.; Tao, Z.; Thirman, J.; Tornai, G. J.; Tsuchimochi, T.; Tubman, N. M.; Veccham, S. P.; Vydrov, O.; Wenzel, J.; Witte, J.; Yamada, A.; Yao, K.; Yeganeh, S.; Yost, S. R.; Zech, A.; Zhang, I. Y.; Zhang, X.; Zhang, Y.; Zuev, D.; Aspuru-Guzik, A.; Bell, A. T.; Besley, N. A.; Bravaya, K. B.; Brooks, B. R.; Casanova, D.; Chai, J.-D.; Coriani, S.; Cramer, C. J.; Cserey, G.; DePrince, A. E.; DiStasio, R. A.; Dreuw, A.; Dunietz, B. D.; Furlani, T. R.; Goddard, W. A.; Hammes-Schiffer, S.; Head-Gordon, T.; Hehre, W. J.; Hsu, C.-P.; Jagau, T.-C.; Jung, Y.; Klamt, A.; Kong, J.; Lambrecht, D. S.; Liang, W.; Mayhall, N. J.; McCurdy, C. W.; Neaton, J. B.; Ochsenfeld, C.; Parkhill, J. A.; Peverati, R.; Rassolov, V. A.; Shao, Y.; Slipchenko, L. V.; Stauch, T.; Steele, R. P.; Subotnik, J. E.; Thom, A. J. W.; Tkatchenko, A.; Truhlar, D. G.; Van Voorhis, T.; Wesolowski, T. A.; Whaley, K. B.; Woodcock, H. L.; Zimmerman, P. M.; Faraji, S.; Gill, P. M. W.; Head-Gordon, M.; Herbert, J. M.; Krylov, A. I. Software for the Frontiers of Quantum Chemistry: An Overview of Developments in the Q-Chem 5 Package. *J. Chem. Phys.* **2021**, *155*, 084801; <https://doi.org/10.1063/5.0055522>.
34. Lin, Y. S.; Li, G.; Mao, S.; Chai, J. D. Long-range Corrected Hybrid Density Functionals with Improved Dispersion Corrections. *J. Chem. Theory Comput.* **2013**, *9*, 263; <https://doi.org/10.1021/ct300715s>.
35. Rohrdanz, M. A.; Herbert, J. M. Simultaneous Benchmarking of Ground-And Excited-State Properties with Long-Range-Corrected Density Functional Theory. *J. Chem. Phys.* **2008**, *129*, 034107; <https://doi.org/10.1063/1.2954017>.
36. Patra, A.; Pipim, G. B.; Krylov, A. I.; Mallikarjun Sharada, S. Performance of Density Functionals for Excited-State Properties of Isolated Chromophores and Exciplexes: Emission Spectra, Solvatochromic Shifts, and Charge-Transfer Character. *J. Chem. Theory Comput.* **2024**. submitted; <https://doi.org/10.1021/acs.jctc.4c00005>.
37. Barone, V.; Cossi, M. Quantum Calculation of Molecular Energies and Energy Gradients in Solution by a Conductor Solvent Model. *J. Phys. Chem. A* **1998**, *102*, 1995; <https://doi.org/10.1021/jp9716997>.
38. Cammi, R.; Mennucci, B. Linear Response Theory for the Polarizable Continuum Model. *J. Chem. Phys.* **1999**, *110*, 9877; <https://doi.org/10.1063/1.478861>.
39. Cossi, M.; Barone, V. Time-dependent Density Functional Theory for Molecules in Liquid Solutions. *J. Chem. Phys.* **2001**, *115*, 4708; <https://doi.org/10.1063/1.1394921>.
40. Luzanov, A. V.; Sukhorukov, A. A.; Umanskii, V. Application of Transition Density Matrix for Analysis of Excited States. *Theor. Exp. Chem.* **1976**, *10*, 354. Russian original: *Teor. Eksp. Khim.*, *10*, 456 (1974); <https://doi.org/10.1007/bf00526670>.
41. B  ppler, S. A.; Plasser, F.; Wormit, M.; Dreuw, A. Exciton Analysis of Many-Body Wave Functions: Bridging the Gap between the Quasiparticle and Molecular Orbital Pictures. *Phys. Rev. A* **2014**, *90*, 052521; <https://doi.org/10.1103/physrev.90.052521>.
42. Plasser, F.; Wormit, M.; Dreuw, A. New Tools for the Systematic Analysis and Visualization of Electronic Excitations. I. Formalism. *J. Chem. Phys.* **2014**, *141*, 024106; <https://doi.org/10.1063/1.4885819>.
43. Plasser, F.; B  ppler, S. A.; Wormit, M.; Dreuw, A. New Tools for the Systematic Analysis and Visualization of Electronic Excitations. II. Applications. *J. Chem. Phys.* **2014**, *141*, 024107; <https://doi.org/10.1063/1.4885820>.
44. Kimber, P.; Plasser, F. Toward an Understanding of Electronic Excitation Energies beyond the Molecular Orbital Picture. *Phys. Chem. Chem. Phys.* **2020**, *22*, 6058; <https://doi.org/10.1039/d0cp00369g>.
45. Mewes, S. A.; Plasser, F.; Krylov, A. I.; Dreuw, A. Benchmarking Excited-State Calculations Using Exciton Properties. *J. Chem. Theory Comput.* **2018**, *14*, 710; <https://doi.org/10.1021/acs.jctc.7b01145>.
46. Plasser, F.; Krylov, A. I.; Dreuw, A. Libwfa: Wavefunction Analysis Tools for Excited and Open-Shell Electronic States. *WIREs: Comput. Mol. Sci.* **2022**, *12*, e1595; <https://doi.org/10.1002/wcms.1595>.
47. Head-Gordon, M.; Grana, A. M.; Maurice, D.; White, C. A. Analysis of Electronic Transitions as the Difference of Electron Attachment and Detachment Densities. *J. Phys. Chem.* **1995**, *99*, 14261; <https://doi.org/10.1021/j100039a012>.
48. Martin, R. L. Natural Transition Orbitals. *J. Phys. Chem. A* **2003**, *118*, 4775; <https://doi.org/10.1063/1.1558471>.
49. Krylov, A. I. From Orbitals to Observables and Back. *J. Chem. Phys.* **2020**, *153*, 080901; <https://doi.org/10.1063/5.0018597>.
50. Gosnell, T. R. *Fundamentals of Spectroscopy and Laser Physics*; Cambridge University Press: Cambridge, UK, 2002.
51. Guiglion, P.; Zwijnenburg, M. A. Contrasting the Optical Properties of the Different Isomers of Oligophenylene. *Phys. Chem. Chem. Phys.* **2015**, *17*, 17854; <https://doi.org/10.1039/c5cp01916h>.
52. Gholami, M.; Tykwinski, R. R. Oligomeric and Polymeric Systems with a Cross-Conjugated  $\pi$ -framework. *Chem. Rev.* **2006**, *106*, 4997; <https://doi.org/10.1021/cr0505573>.
53. Fujiwara, H.; Kitamura, T.; Wada, Y.; Yanagida, S.; Kamat, P. V. Onium Salt Effects on P-Terphenyl-Sensitized Photoreduction of Water to Hydrogen. *J. Phys. Chem. A* **1999**, *103*, 4874; <https://doi.org/10.1021/jp984740u>.
54. Hansch, C.; Leo, A.; Taft, R. W. A Survey of Hammett Substituent Constants and Resonance and Field Parameters. *Chem. Rev.* **1991**, *91*, 165; <https://doi.org/10.1021/cr00002a004>.

**Supplementary Material:** This article contains supplementary material (<https://doi.org/10.1515/pac-2025-0560>).